Electronic Supplementary Information For:

Fine-tuning Conjugation in Polyoxometalate Non-Linear Optical Chromophores: A Molecular Electronic "Goldilocks" Effect

Ahmed Al-Yasari, Philip Spence, Hani El Moll, Nick Van Steerteghem, Peter. N. Horton, Bruce S. Brunschwig, Koen Clays and John Fielden

General

Materials and Procedures. Tetrahydrofuran (THF), acetonitrile (MeCN) and dimethylformamide (DMF) were freshly distilled under nitrogen from an appropriate drying agent.[1] Dry (sure seal) dimethyl sulfoxide (DMSO) was purchased from Sigma Aldrich. All other reagents and solvents were obtained as ACS grade from Sigma Aldrich, Alfa Aesar or Fisher Scientific and used as supplied. Tetrabutylammonium hexamolybdate[2] was synthesized according to previously published methods. 4-{[4-(9H-carbazol-9-yl)phenyl]ethynyl}aniline (**P2**) was following synthetic route shown in Scheme S1. 4-[(4-aminophenyl)ethynyl]-N,N-diphenylaniline (**P3)** was synthesized via Sonogashira coupling between 4-bromotriphenylamine and 4-ethynylaniline, as shown in Scheme S1. Organoimido hexamolybdate derivatives were synthesised using an adapted literature procedure,[3] under an atmosphere of dry nitrogen using standard schlenk techniques.

Physical Measurements. FT-IR spectra were measured using Perkin Elmer FT-IR spectrum BX and Bruker FT-IR XSA spectrometers. ^{1}H- and ^{13}C-NMR spectra were acquired using Bruker AC 300 (300 MHz) and Bruker Ascend 500 (500 MHz) spectrometers and all shifts are quoted with respect to TMS using the solvent signals as secondary standard (s = singlet, d = doublet, t = triplet, q = quartet, sex = sextet, dt = doublet of triplets, m = multiplet). Quaternary carbon signals were not observed for these compounds even after 1064 scans of saturated d_6-DMSO solutions, which gave strong signal for all other ^{13}C resonances. Elemental analyses and accurate mass spectrometry were outsourced to London Metropolitan University, and the UK National Mass Spectrometry Service at Swansea University respectively. UV–Vis spectra were obtained by using an Agilent Cary 60 UV-Vis spectrophotometer. Cyclic voltammetric measurements were carried out using Autolab PGStat 30 potentiostat/galvanostat. A single-compartment or a conventional three-electrode cell was used with a silver/silver chloride reference electrode (3M NaCl, saturated AgCl), glassy carbon or platinum working electrode and Pt wire auxiliary electrode. Acetonitrile was freshly distilled (from CaH_2), $[N(C_4H_9\text{-}n)_4]PF_6$, as supplied from Fluka, and $[N(C_4H_9\text{-}n)_4]BF_4$,[4] was used as the supporting electrolyte. Solutions containing ca. 10^{-3} M analyte (0.1 M electrolyte) were degassed by purging with nitrogen. All $E_{1/2}$ values were calculated from $(E_{pa} + E_{pc})/2$ at a scan rate of 100 mV s^{-1} and referenced to Fc/Fc^{+}.

Synthetic Methods

Summary. Our synthetic approach is summarized in Scheme S1. Hexamolybdate derivatives were obtained through DCC-mediated coupling of anilines with hexamolybdate, using an excess (1.3 equivalents) of $(NBu_4)_2[Mo_6O_{19}]$ to prevent formation of *bis*-imido products. Standard carbon-carbon and N-aryl coupling methods were used to access the precursor anilines **P1** to **P3**. We found that synthesis of the complete ligands was a more effective approach than the Sonogashira coupling of $[Mo_6O_{18}NPhI]^{2-}$ with appropriate alkynes (used for related compounds in our previous work[5]). This may be because both **1** and **2** seem more moisture sensitive than other arylimido-POMs and may not tolerate the Sonogashira conditions.

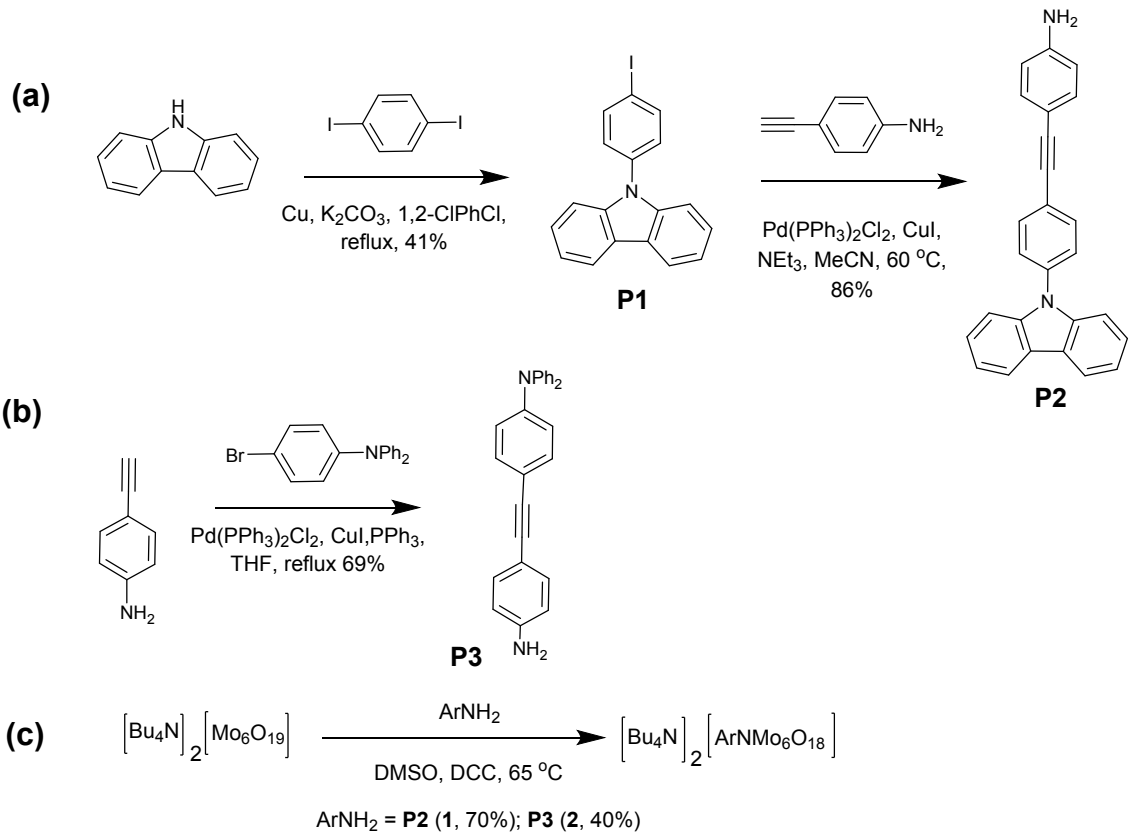

Scheme S1 Synthetic approach to **(a)** 4-{[4-(9H-carbazol-9-yl)phenyl]ethynyl}aniline (**P2**); **(b)** 4-[(4-aminophenyl)ethynyl]-N,N-diphenylaniline (**P3**); and **(c)** Arylimido-polyoxometalates (POMophores) **1** and **2**.

Synthesis of 9-(4-iodophenyl)-9H-carbazole (P1). A mixture of carbazole (2 g, 12mmol), 1,4-diiodobenzene (6 g, 19.6 mmol), copper powder (1.2 g, 18.88 mmol) and potassium carbonate (2.4 mg, 17.36 mmol) was dissolved in 1,2-dichlorobenzene (32 mL) and refluxed at 180 ºC for 48 hrs. The solution was taken and concentrated on the rotary evaporator before isolating the product by Kugelrohr distilling out unreacted carbazole at 280 ºC. The remaining product was then recrystallized in hot acetone to give a creamy coloured solid (1.81 g, 4.92 mmol, 41 %). δ_H (500 MHz, $(CD_3)_2SO$) 8.25 (d, J = 7.7 Hz, 2H), 8.02 (d, J = 8.5 Hz, 2H), 7.46 (d, J = 8.5 Hz, 2H), 7.44 - 7.26 (m, 6H). δ_C (125 MHz, $(CD_3)_2SO$) 134.2, 139.5, 137.1, 129.4, 126.8, 123.3, 121.8, 120.8, 110.0, 93.5. m/z = 370 $[C_{18}H_{12}INH]^+$. FTIR (ATR)/cm^{-1}: 3044 (sh); 1622 (vw); 1595 (m); 1580 (m); 1151 (m); 1494 (s); 1479 (s); 1449 (vs); 1361 (m); 1335 (s); 1316 (s); 1293 (w); 1229 (vs); 1183 (m); 1121 (m); 1101 (w); 1005 (w); 934 (m); 913 (w); 855 (w); 823 (s); 747 (vs); 723 (vs); 707 (m); 634 (m); 617 (m).

Synthesis of 4-{[4-(9H-carbazol-9-yl)phenyl]ethynyl}aniline (P2). **P1** (300 mg, 0.8 mmol), 4-ethynylaniline (112 mg, 0.96 mmol), copper iodide powder (3.8 mg, 0.02 mmol) and $Pd(PPh_3)_2Cl_2$ (56 mg, 0.08 mmol) were dissolved in acetonitrile (10 mL) and triethylamine (0.1 mL, 0.072 mmol) was added. The solution was stirred for 24 hrs at 60 ºC. The reaction mixture was filtered and washed with water (2 × 10 ml), and then DCM (2 × 10 mL).The combined organic layers were dried over $MgSO_4$ and concentrated on the rotary evaporator to give the crude product as red solid which was purified by silica gel column chromatography (Hexane:DCM, 1:2 ratio) to afford the desired product as yellow solid (0.246 g, 0.686 mmol, 86 %). δ_H (300 MHz, $(CD_3)_2SO$) 8.26 (d, J =7.7 Hz, 2H), 7.74 (d, J =8.3 Hz, 2H), 7.64 (d, J = 8.3 Hz, 2H), 7.50-7.23 (m, 6H), 7.26 (d, J = 8.5 Hz, 2H), 6.59 (d, J = 8.5 Hz, $2H_j$), 5.64 (s, 2H). δ_C (125 MHz, $(CD_3)_2SO$) 149.7, 139.9, 136.1, 132.7, 132.6, 126.8, 126.4, 122.9, 122.5, 120.6, 120.3, 113.6, 109.7, 107.8, 92.3, 86.0. Anal. Calcd (found) % for $(C_{26}H_{18}N_2)_{0.87}(CH_2Cl_2)_{0.13}$: C, 84.62 (84.51); H, 4.96 (4.51); N, 7.54 (7.80). m/z = 359 $[C_{26}H_{18}N_2H]^+$. FTIR (ATR)/cm^{-1}: 3458 (m);

3366 (m); 3206 (vw); 3040 (w); 2207 (m); 1620 (s); 1602 (s); 1518 (s); 1476 (m); 1446 (s); 1334 (m); 1312 (m); 1286 (m); 1222 (s); 1169 (s); 1136 (m); 1014 (vw); 912 (m); 826 (vs); 751 (vs); 724 (s); 645 (s); 623 (m). UV-vis (MeCN) λ, nm (ε, M^{-1} cm^{-1}): 234 (39500), 292.5 (31300), 339.5 (46200).

Synthesis of 4-[(4-aminophenyl)ethynyl]-N,N-diphenylaniline (P3). A dried 50 ml two neck round flask was charged with 4-bromotriphenylamine (324 mg, 1 mmol), 4-ethynylaniline (140 mg, 1.2 mmol), copper iodide powder (4.8 mg, 0.025 mmol), $Pd(PPh_3)_2Cl_2$ (70 mg, 0.1 mmol) and triphenylphosphine (131 mg, 0.5 mmol) and then evacuated and filled with Ar (× 3). THF (10 mL) was added to the mixture and the solution was refluxed for 96 hrs. The solution was filtered, then washed with water (10 mL) and (3 × 15 mL) DCM. The organic layer was taken and dried with magnesium sulphate before being concentrated *in vacuo*. The product was then purified by silica column chromatography using hexane:DCM; 1:2 to afford a light-red solid (0.25 g, 0.69 mmol, 69 %). δ_H (500 MHz, $(CD_3)_2SO$) 7.35 (d, 2H, J = 8.8 Hz), 7.33 (m, 4H), 7.15 (d, J = 8.6 Hz, 2H), 7.08 (m, 6H), 6.89 (d, J = 8.8 Hz, 2H), 6.54 (d, J = 8.6 Hz, 2H), 5.51 (s, 2H). δ_C (125 MHz, $(CD_3)_2SO$) 149.2, 146.8, 146.6, 132.4, 132.0, 129.70, 124.7, 123.8, 121.9, 116.4, 113.6, 108.5, 90.3, 86.5. Anal. Calcd (found) % for $C_{26}H_{20}N_2$: C, 86.62 (86.73); H, 5.59 (5.67); N, 7.77 (7.63). *m/z* = 361 $[C_{26}H_{20}N_2H]^+$. FTIR (ATR)/cm^{-1}: 3481 (vw); 3390 (w); 2198 (vw); 1613 (m); 1586 (m); 1517 (m); 1486 (s); 1319 (m); 1275 (s); 1176 (m); 1153 (w); 1075 (w); 1012(w); 824 (s); 757 (s); 721 (s); 693 (s); 616 (s); 517 (vs). UV-vis (MeCN) λ, nm (ε, M^{-1} cm^{-1}): 205.0 (57500), 233.5 (12700), 348.0 (41100).

Synthesis of $[(C_4H_9)_4N]_2[Mo_6O_{18}N_2C_{26}H_{16}]$ (1). 4-{[4-(9H-carbazol-9-yl)phenyl]ethynyl}aniline (**P2**) (0.359 g, 1 mmol), $(n\text{-}Bu_4N)_2[Mo_6O_{19}]$, (1.773 g, 1.3 mmol), and DCC (1,3-dicyclohexylcarbodiimide) (0.237 g, 1.15 mmol) were heated in dry DMSO (15 mL) for 12 h at 65 ºC. The colour of the solution changed to red while it was heated. After cooling to room temperature, the solution was filtered into a flask containing diethyl ether (200 mL) and ethanol (50 mL) resulting in an orange precipitate. The latter was washed with ethanol (10 mL) and ether (10 mL) several times, then recrystallized twice from hot acetonitrile and washed with ethanol (10 mL) and diethyl ether (10 mL) to afford orange crystals (1.19g, 0.549 mmol, 70 %). δ_H (500 MHz, CD_3CN) 8.20 (d, J = 7.7 Hz, 2H), 7.81 (d, J = 8.6 Hz, 2H), 7.66 (d, J = 8.6 Hz, 2H), 7.61 (d, J = 8.6 Hz, 2H), 7.46 (m, 4H), 7.32 (m, 2H), 7.26 (d, J = 8.6 Hz, 2H), 3.10 (*p*t, J = 8.6 Hz, 16H), 1.61 (quin, J = 8.0 Hz, 16H), 1.36 (sex, J = 7.4 Hz, 16H), 0.97 (t, J = 7.4 Hz, 24H). δ_C (125 MHz, CD_3CN) 141.5, 134.3, 132.8, 128.1, 127.3, 127.2, 126.6, 124.4, 123.2, 122.6, 121.4, 110.9, 59.4, 24.4, 20.4, 13.9. Anal. Calcd (found) % for $C_{58}H_{88}N_4Mo_6O_{18}$: C, 40.85 (40.93); H, 5.20 (5.13); N, 3.28 (3.30). *m/z* = 610.2 $[C_{26}H_{16}N_2Mo_6O_{18}]^{2-}$. FTIR (ATR)/$cm^{-1}$: 2960 (m); 2873 (m); 2162 (vw); 1625 (vw); 1597 (w); 1513 (m); 1479 (m); 1449 (s); 1378 (w); 1334 (m); 1229 (m); 1169 (w); 1150 (w); 1103 (w); 1062 (w); 1014 (w); 975 (s); 947 (vs); 880 (w); 845 (m); 775 (vs); 749 (vs); 723 (s). UV-vis (MeCN) λ, nm (ε, M^{-1} cm^{-1}): 226.5 (70400); 291.5 (48400); 326.5 (31300); 341 (33700); 384.5 (43400).

Synthesis of $[(C_4H_9)_4N]_2[Mo_6O_{18}N_2C_{26}H_{18}]$ (2). A mixture of 4-[(4-aminophenyl)ethynyl]-N,N-diphenylaniline (**P3**) (0.36 g, 1 mmol), $(n\text{-}Bu_4N)_2[Mo_6O_{19}]$ (1.773 g, 1.3 mmol), and DCC (1,3-dicyclohexylcarbodiimide) (0.237 g, 1.15 mmol) was heated in dry DMSO (15 mL) for 10 h at 68 ºC. After cooling to room temperature, the solution was filtered into a flask containing diethyl ether (200 mL) and ethanol (50 mL) and left to stand for 4 hours resulting in a red sticky precipitate. This was washed with ethanol (10 mL) and ether (10 mL) several times before being recrystallized twice from hot acetonitrile and washed with ethanol (10 mL) and diethyl ether (10 mL) to give red crystals (0.68g, 0.5 mmol, 40 %). δ_H (500 MHz, CD_3CN) 7.50 (d , J = 8.3 Hz, 2H), 7.38 (d, J = 8.5 Hz, 2H), 7.33 (t, J = 7.8 Hz, 4H), 7.22 (d, J = 8.3 Hz, 2H), 7.12 (m, 6H), 6.94 (d, J = 8.5 Hz, 2H), 3.09 (*p*t, J = 8.6 Hz, 16H), 1.60 (quint, J = 8.0 Hz, 16H), 1.36 (sex, J = 7.4 Hz, 16H), 0.97 (t, J = 7.3 Hz, 24H). δ_C (125 MHz, CD_3CN) 148.2, 133.9, 132.6, 130.9, 127.4, 126.5, 125.3, 124.1, 122.7, 116.1, 94.0, 89.0, 59.6,

24.6, 20.6, 14.0. Anal. Calcd (found) % for $C_{58}H_{90}N_4Mo_6O_{18}$: C, 40.80 (40.71); H, 5.31 (5.43); N, 3.28 (3.28). *m/z* = 611 $[C_{26}H_{18}N_2Mo_6O_{18}]^{2-}$. FTIR (ATR)/$cm^{-1}$: 2960 (m); 2872 (m); 2201 (vw); 1581 (m); 1507 (m); 1482 (s); 1379 (w); 1331 (m); 1168 (vw); 1136 (vw); 1100(vw); 1057 (vw); 1028 (vw); 974 (s); 945 (vs); 881 (w); 843 (w); 770 (vs); 696 (s). UV-vis (MeCN) λ, nm (ε, M^{-1} cm^{-1}): 292.0 (41200); 326.5 (36200); 414.0 (45300).

UV-visible Spectra

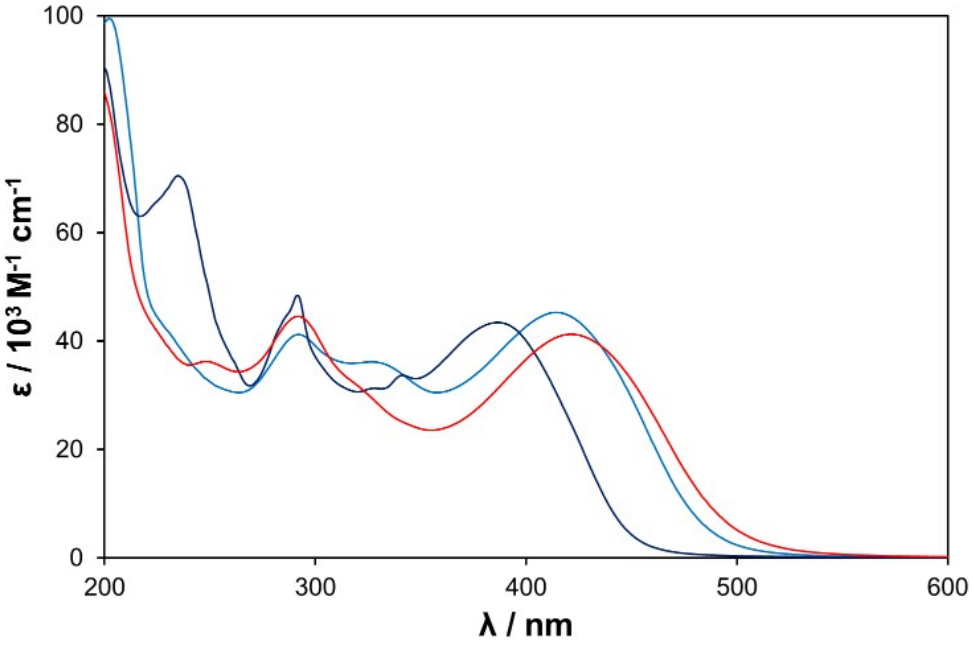

Fig. S1 UV-visible spectra of **1** (dark blue), **2** (blue) and **3** (red), obtained in acetonitrile at 298 K.

X-ray Crystallographic Details

Sample Growth, Data Collection and Refinement. Crystals of **1** and **2**·0.25MeCN were obtained by room temperature diffusion of diethyl ether vapour into acetonitrile. The structure of **3** has previously been published. Data were collected on Oxford Diffraction XCalibur 3 diffractometer, or a Rigaku AFC 12 goniometer equipped with an enhanced sensitivity (HG) Saturn724+ detector and FR-E+ SuperBright molybdenum rotating anode generator with HF Varimax optics (100 μm focus). Data reduction, cell refinement and absorption correction was carried out using Agilent Technologies CrysAlisPro[6] or Rigaku CrystalClear-SM Expert software,[7] and solved using SHELXS-2014[8] *via* WinGX[9] or OLEX2.[10] Refinement was achieved by full-matrix least-squares on all F_0^2 data using SHELXL-2014[11] and molecular graphics were prepared using ORTEP-3.[12] Both **1** and **2**·0.25MeCN showed disorder requiring the use of restraints on thermal parameters and certain bond distances, for **1** this included restraining the carbon atoms of the phenyl groups to a regular hexagon. In **2**·0.25MeCN there is substantial solvent accessible void space, likely to be occupied by disordered MeCN – however this was not located and refined. Full crystallographic data and refinement details are presented in Table S1. In **1** the asymmetric unit contains the complete molecular anion and both cations, while in **2** there are two crystallographically independent anions, and four crystallographically independent $[NBu_4]^+$ cations. See Figure S2 and S3.

Table S1. Crystallographic Data and Refinement Details for **1** and **2**.

	1	**2**·0.25MeCN
Formula	$C_{58}H_{88}Mo_6N_4O_{18}$	$C_{58.5}H_{90.75}Mo_6N_{4.25}O_{18}$
M	1704.96	1717.24
cryst syst	Monoclinic	Orthorhombic
space group	$P2_1/c$	*P*na21
a/Å	11.8775(4)	16.7634(2)
b/Å	19.8944(9)	32.5035(4)
c/Å	28.8944(2)	30.9114(6)
α/deg	90	90
β/deg	101.088(4)	90
γ/deg	90	90
U/Å^3	6701.3(5)	16842.7(4)
Z	4	8
T/K	140(2)	100(2)
μ/mm^{-1}	1.157	0.921
Cryst. size/mm	0.45 × 0.3 × 0.08	0.20 × 0.09 × 0.07
Cryst. description	Orange plate	Orange block
No. reflns collected	140513	165986
No. of indep. reflns (R_{int})	15346 [R(int) = 0.1127]	38580 [R(int) = 0.0376]
θ_{max}/deg (completeness)	99.9%	99.9 %
Reflections with $I > 2\sigma(I)$	7508	32626
Goodness-of-fit on F^2	1.022	1.088
Flack parameter	N/A	-0.03(1)
final R_1, wR_2 [$I > 2\sigma(I)$][a]	R1 = 0.1103, wR2 = 0.2707	R1 = 0.0699, wR2 = 0.2080
(all data)	R1 = 0.1866, wR2 = 0.3278	R1 = 0.0807, wR2 = 0.2178
Peak and hole/e Å^{-3}	1.785 and -0.925	1.214 and -0.791

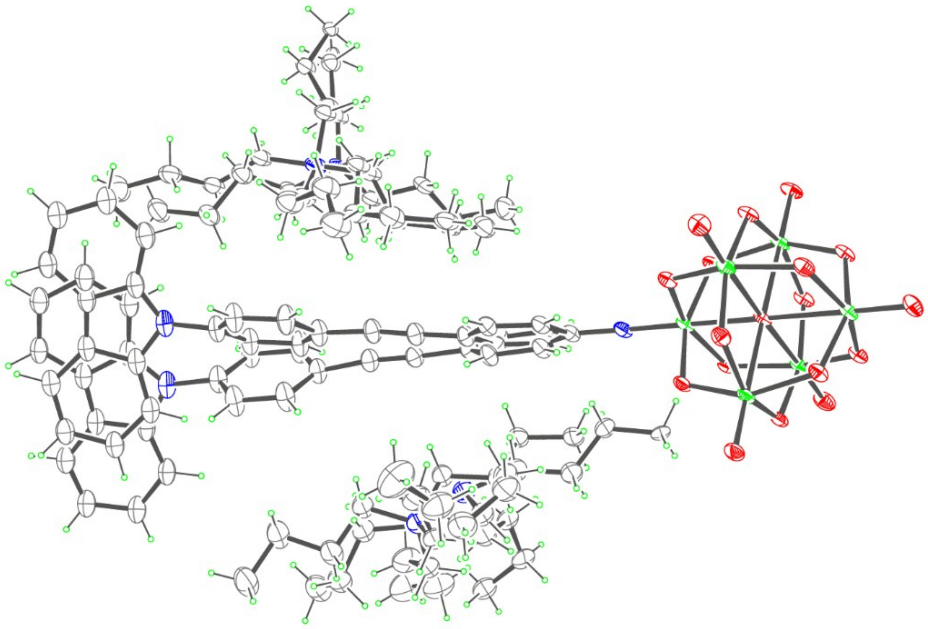

Fig. S2 ORTEP representation of the asymmetric unit in **1**. Thermal ellipsoids are at the 10% probability level. Colour scheme: Mo is green; O, red; C, gray; N, blue; H atoms are represented by green circles of arbitrary radii.

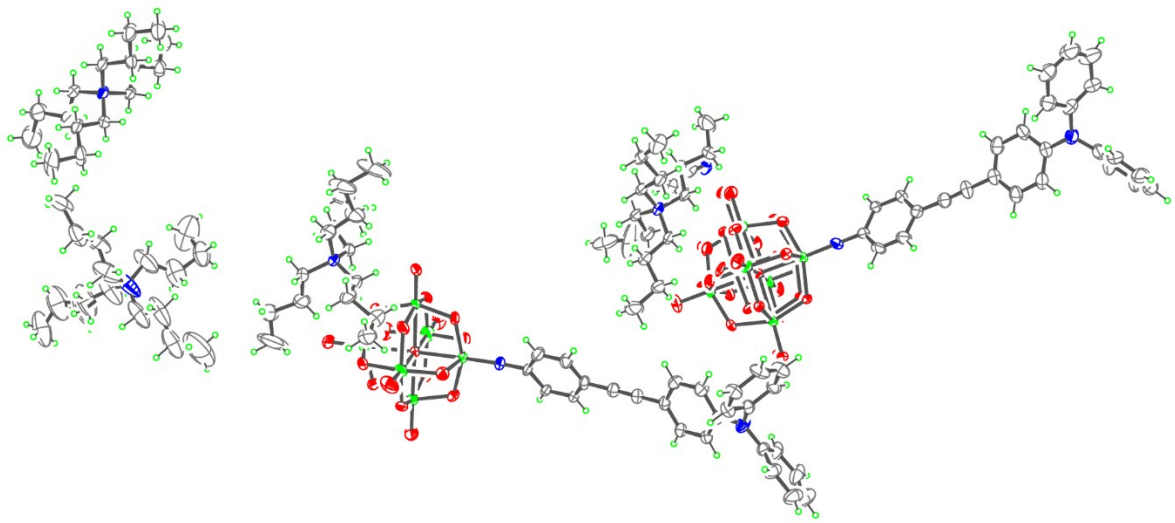

Fig. S3 ORTEP representation of the asymmetric unit in **2**. Thermal ellipsoids are at the 10% probability level. Colour scheme as Fig. S1.

Hyper-Rayleigh Scattering

General details of the hyper-Rayleigh scattering (HRS) experiment have been discussed elsewhere,[13] and the experimental procedure and data analysis protocol used for the fs measurements used in this study were as previously described.[14] Measurements were carried out using dilute (*ca.* 10^{-5} M) filtered (Millipore, 0.45 μm) acetonitrile solutions, such that self-absorption of the SHG signal was negligible, verified by the linear relation between signal and concentration. Measurements at both 1064 and 1100 nm were carried out in acetonitrile, using a Spectra-Physics InSight® DS+ laser (1W average power, sub-100 fs pulses, 80 MHz). In this setup, the collection optics are coupled to a spectrograph (model Bruker 500is/sm), together with an EMCCD camera (Andor Solis model iXon Ultra 897). Correction for multiphoton induced fluorescence was done by subtracting the broad MPF background signal from the narrow HRS peak (FWHM ± 9 nm). The higher accuracy of this setup enables us to use the solvent as an internal reference (acetonitrile, $\beta_{HRS,1064} = 0.258 \times 10^{-30}$ esu; $\beta_{zzz,1064} = 0.623 \times 10^{-30}$ esu).[15]

Stark Spectroscopy

Stark spectra were collected in butyronitrile glasses at 77 K (estimated local field correction $f_{int} = 1.33$). Apparatus and data collection procedure were as previously reported,[16] but with a Xe arc lamp as the light source in place of a W filament bulb. Each spectrum was measured at least twice, and spectra were modelled with a sum of three or four Gaussian curves that reproduce the band of interest. The 2nd derivatives of the Gaussian curves were then used to fit the Stark spectra with Liptay's equation.[17] The dipole moment change $\Delta\mu_{12} = \mu_e - \mu_g$ (where μ_e and μ_g are the respective excited and ground state dipole moments) was then calculated from the coefficient of the second derivative component. This assumes that the two-state model is applicable to the systems investigated here – which at higher transition energies in particular may be complicated from mixing with other states close in energy. Thus, values obtained for the highest energy absorption bands are subject to additional uncertainty.

A two-state analysis of the ICT transitions gives

$$\Delta\mu_{ab}^2 = \Delta\mu_{12}^2 + 4\mu_{12}^2 \qquad (1)$$

where $\Delta\mu_{ab}$ is the dipole moment change between the diabatic states, $\Delta\mu_{12}$ is the observed (adiabatic)

dipole moment change, and μ_{12} is the transition dipole. The value of μ_{12} can be determined from the oscillator strength f_{os} of the transition by

$$|\mu_{12}| = \left(\frac{f_{os}}{1.08 \times 10^{-5} E_{max}} \right)^{1/2} \quad (2)$$

where E_{max} is the energy of the ICT maximum (in wavenumbers) and μ_{12} is in eÅ. The latter is converted into Debye units upon multiplying by 4.803. The degree of delocalization c_b^2 and electronic coupling matrix element H_{ab} for the diabatic states are given by

$$|H_{ab}| = \left| \frac{E_{max}(\mu_{12})}{\Delta\mu_{ab}} \right| \quad (3)$$

$$c_b^2 = \frac{1}{2} \left| 1 - \left(\frac{\Delta\mu_{12}^2}{\Delta\mu_{12}^2 + 4\mu_{12}^2} \right)^{1/2} \right| \quad (4)$$

If the hyperpolarizability tensor β_0 has only nonzero elements along the ICT direction, then this quantity is given by

$$\beta_0 = \frac{3\Delta\mu_{12}(\mu_{12})^2}{(E_{max})^2} \quad (5)$$

The Gaussian fitting procedure used for the Stark spectra depends on a variety of parameters as well as the choice of baseline. Previously, for spectra fitted with three Gaussian curves and all three derivatives, we estimated a precision for calculated β_0 values of *ca.* ±20% given a consistent fitting approach.[5b] However, the actual error of the fitted parameters versus their true values is difficult to estimate, and likely larger. In this study, use of a fourth Gaussian curve is expected to increase errors, while our ability to obtain satisfactory fits using only the 2nd derivative component should reduce them. Thus, as before, the experimental errors for μ_{12}, $\Delta\mu_{12}$ are estimated to be ±20%. Errors for $\Delta\mu_{ab}$, H_{ab} and c_b^2 are estimated as ±30, ±30 and ±50%, respectively.

The fits obtained are shown overleaf. As stated above, in previous work on **3** and related compounds,[5b] we fitted the Stark spectra to the 2nd, 1st and 0th derivatives of the Gaussian curves used to fit the absorption spectra. The use of a 4th Gaussian to model the absorption spectra of **1** and **2** led us to fit with only the 2nd derivative, to avoid over-parameterisation. To ensure comparability, **3** has been fitted with the same 2nd derivative only approach, producing almost no change in the values previously published – a 4 Gaussian fit of **3** was also tested and found to be no different as the additional Gaussian curve became vanishingly small. A satisfactory fit of **1** can also be produced using only three Gaussian curves, yielding a lower (by *ca.* 10%) $\Sigma\beta_0$, however the 4 Gaussian fit is presented here for comparability with that of **2**.

For the purposes of the discussion in the main paper, $\Delta\mu_{12}$ is the dipole moment change used to calculate β_0 and relates only to the dipolarity of the electronic transitions, whereas $\Delta\mu_{ab}$ also has dependence on μ_{12} which relates to the strength of the transitions. Multiplying either of these $\Delta\mu$ values by the electron angstrom (0.20819434 eÅ) converts it to the respective charge transfer (CT) distance – delocalized r_{12} or localized r_{ab}. Of these r_{ab} should relate more closely to actual geometric CT distances, but both are always much smaller than crystallographically observed donor-acceptor distances. The transition dipole μ_{12} and oscillator strength f_{os} indicate the strength of the electronic transitions. H_{ab} indicates the strength of donor-acceptor electronic coupling (higher values mean stronger coupling). c_b^2 provides information on delocalization – a value of 0.5 indicates complete delocalization, while values of 1 or 0 indicate no delocalization.

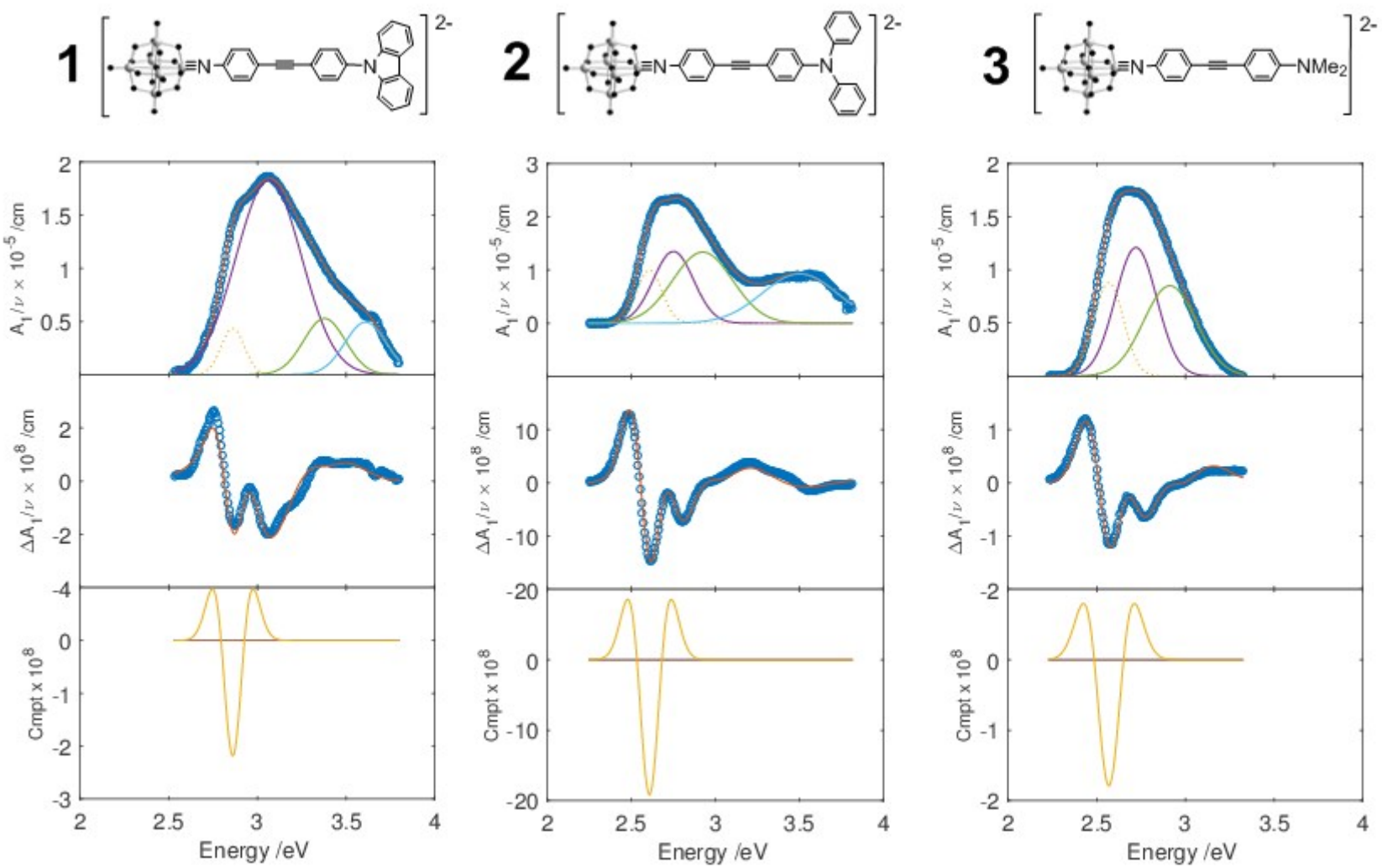

Fig. S4 Stark spectra and fits for **1** to **3** at 77 K. **Top** – absorption spectrum (blue circles), fit (red line) and contributing Gaussian curves (purple, yellow, green); **Middle** – Stark spectrum (blue circles), fit (orange line); **Bottom** – Overall contribution of derivatives. In these cases, only the second derivative has been allowed to contribute.

DFT calculations

Method. DFT calculations were carried out using the ADF suite of programs.[18] Geometry optimsation was carried out using the ADF triple-ζ TZP basis set with the zero-order regular approximation (ZORA) to account for relativitstic effects.[19] A 'small' frozen core was employed for the molybdenum atoms. The generalized-gradient approximation (GGA) was employed in the geometry optimizations using the Beck and Perdew (BP86) exchange-correlation (XC) functional.[20,21] Calculations of the polarizability, second-order polarizability and electronic spectra used the RESPONSE and EXCITATION modules implemented in the ADF program[22] and were based on the optimized geometries. TD-DFT with the SAOP XC and ADF triple-ζTZ2P basis set with no frozen core were used for these calculations.[23] Solvent (acetonitrile) was introduced using COSMO with Klamt atomic Radii. The subkey NOCSMRSP was applied to prevent induced electronic charges from influencing COSMO surface charges, together with the ALLPOINTS key. Without NOCSMRSP, calculated β_0 values can be around three times larger.

We have found that lower (and thus more experimentally realistic) β-values can be obtained by performing these calculations with less polar solvent media (e.g. THF), and also by using twisted rather than energy-minimised planar conformations of the diphenylacetlyene bridge.[5b] This suggests that current solvation methods may overestimate the strength of interaction of these POM hybrids with the solvent, and that conformational averaging could be required to produce quantitatively accurate predictions. Such approaches are the subject of ongoing work. On the other hand, using a larger basis set (QZ4P) makes these calculations more expensive, while yielding practically identical results to TZ2P, and the hybrid functional B3LYP with solvation was found to be too computationally expensive to be viable with our set up (quad-core desktop PC, with 16 Gb RAM and Solid-State Drive). In any case, prior gas phase work[24] has found that functionals LC-BLYP, CAM-B3LYP and B3LYP yield very similar results to LB94 – a closely related antecedent to SAOP used here. Lastly, it should be noted that the obtained β values are also provided divided in two in the ADF output files, as this often corresponds better to experimental conventions. If these halved values are used, the orientationally averaged $\beta_{vec,0}$ values obtained by TD-DFT are only *ca.* 2 × larger than the Stark derived β_0. However, we do not take this step and report using the normal theoretician's convention for small molecules.[25]

Results. TD-DFT-calculated $\beta_{zzz,0}$ and orientationally averaged $\beta_{vec,0}$ values are displayed below in Table S2. Table S2 also shows the result of normalising β_0 values for DFT, plus the two experimental techniques to that of **2** as 100%. This makes it very clear that the enhancement from **1** to **3** and then **2** is very similar for TD-DFT, Stark and HRS.

Table S2 TD-DFT calculated β_0-values for **1** to **3** in MeCN and comparison of normalised experimental and TD-DFT calculated β_0.

Compound	**TD-DFT Calculated β_0-values**		**Normalised β_0-values**		
	$\beta_{zzz,0}$ (10^{-30} esu)	$\beta_{vec,0}$ (10^{-30} esu)	HRS	Stark	TD-DFT
1	960	575	42% [a]	51%	44%
2	2160	1293	100% [b]	100%	100%
3	1300	782	71% [b]	80%	60%

[a] From 1100 nm data, considered most reliable for this compound. [b] From 1064 nm data.

The tables S3 to S5 on the following pages summarise the TD-DFT calculated UV-visible spectra for **1** to **3**, together with the contributing orbital-to-orbital transitions and representations of the orbitals involved (Fig. S5 to S7). A brief analysis of the transitions is included below the figures and tables for each compound. These suggest that, overall, **3** has the largest proportion (in terms of total oscillator

strength f_{os}) of highly dipolar transitions, followed by **2**, and that the most significant group of transitions for **1** (in terms of total f_{os}) have little dipolar character as they are between donor and acceptor orbitals that are both spread across a large portion of the molecular hybrid. A key difference between **3** and **2** is the increased strength and lowered energy of the imido-phenyl/bridge-to-POM transition in **2** (HOMO-9 to LUMO+1 in **2**, HOMO-5 to LUMO+7 in **3**), that appears to have significant dipolar charge transfer character. These observations – namely more dipolar transitions in **2** and **3** than in **1** (and possibly in **2** than **3**), coupled with strengthening and lowering in energy of a moderately dipolar transition in **2** *vs* **3**, are very consistent with the Stark measurements.

Table S3 Calculated Gas Phase Electronic Transitions of Compound **1**

Transition Energy / eV	f_{os}	**Normalised f_{os}**[a]	**Orbital contributions**[b]
1.62	0.1397	0.0743	HOMO → LUMO+6 (90%; 0.067)
2.12	0.3298	0.1755	HOMO-1 → LUMO+6 (39%; 0.068) HOMO → LUMO+8 (29%; 0.051) HOMO-1 → LUMO+8 (22%; 0.0386)
2.66	0.2146	0.1142	HOMO → LUMO+15 (24%; 0.027) HOMO-1 → LUMO+8 (21%; 0.024) HOMO-1 → LUMO+12 (13%; 0.015) HOMO-3 → LUMO+2 (13%; 0.015) HOMO-1 → LUMO+10 (9%; 0.010)
2.76	0.6324	0.3366	HOMO → LUMO+15 (59%; 0.199) HOMO-1 → LUMO+8 (19%; 0.064) HOMO-1 → LUMO+15 (6%; 0.020)
2.93	0.1281	0.0681	HOMO-3 → LUMO+6 (84%; 0.057)
3.16	0.1840	0.0979	HOMO-1 → LUMO+15 (77%; 0.075) HOMO-3 → LUMO+8 (5%; 0.005)
3.18	0.2502	0.1332	HOMO → LUMO+18 (71%; 0.094) HOMO-3 → LUMO+8 (15%; 0.02)

[a] f_{os} normalised to the sum of the f_{os} all of the calculated transitions as 1. [b] Significant contributing orbital-to-orbital transitions with weighting (% and normalised f_{os}).

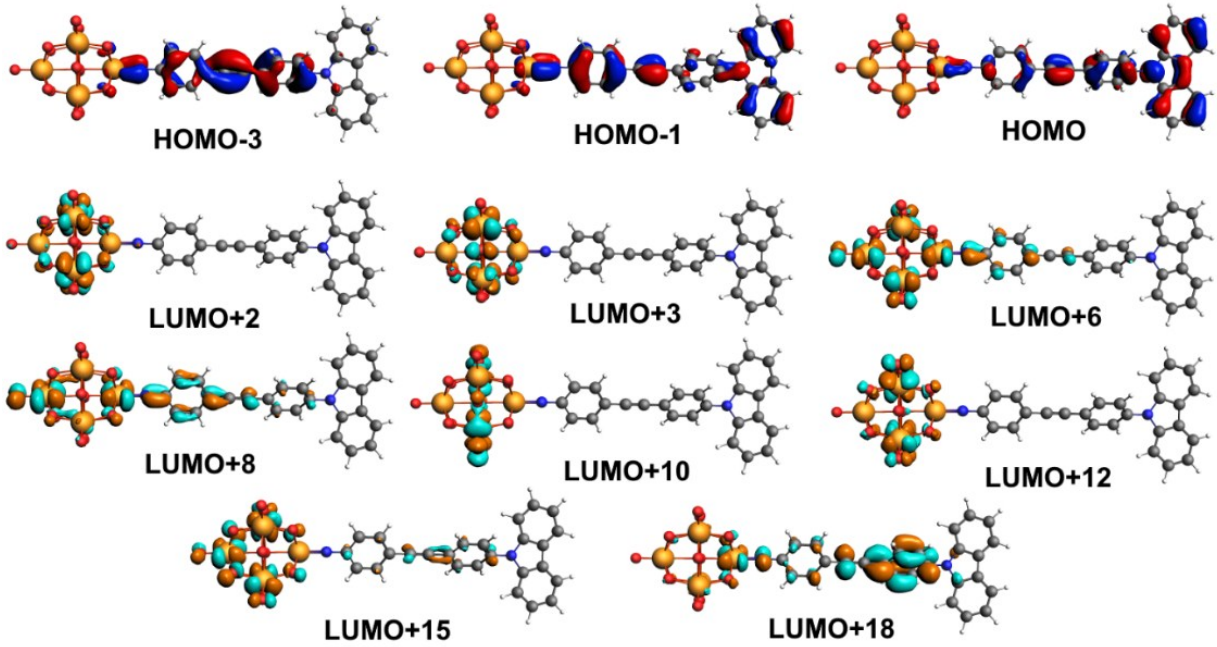

Fig. S5 Orbitals involved in the UV-vis transitions of compound **1**.

Analysis of Table S3 and Fig. S3 reveals three groups of transitions:
Organic (inc. bridge)-to-POM: Highly dipolar but weak, total normalised f_{os} = 0.04
Organic (inc. bridge)-to-POM/imido-aryl: Significant dipolar character, strong, total normalised f_{os} = 0.394
Organic (inc. bridge) to spatially diffuse POM/imido/organic orbitals: Little dipolar character, strong, total normalised f_{os} = 0.455.

Table S4 Calculated Gas Phase Electronic Transitions of Compound **2**

Transition Energy / eV	f_{os}	**Normalised f_{os}**[a]	**Orbital contributions**[b]
1.32	0.1734	0.1000	HOMO → LUMO+6 (94%; 0.094)
1.76	0.2256	0.1301	HOMO → LUMO+8 (90%; 0.112)
2.08	0.2268	0.1308	HOMO-1 → LUMO+6 (78%; 0.102) HOMO-1 → LUMO+8 (17%; 0.022)
2.69	0.9507	0.5484	HOMO-1 → LUMO+8 (38%; 0.208) HOMO-9 → LUMO+1 (30%; 0.165) HOMO-1 → LUMO+10 (5%; 0.027)
3.15	0.1571	0.0906	HOMO-1 → LUMO+15 (68%; 0.062) HOMO-2 → LUMO+8 (8%; 0.007) HOMO-1 → LUMO+17 (6%; 0.005)

[a] f_{os} normalised to the sum of the f_{os} all of the calculated transitions as 1. [b] Significant contributing orbital-to-orbital transitions with weighting (% and normalised f_{os}).

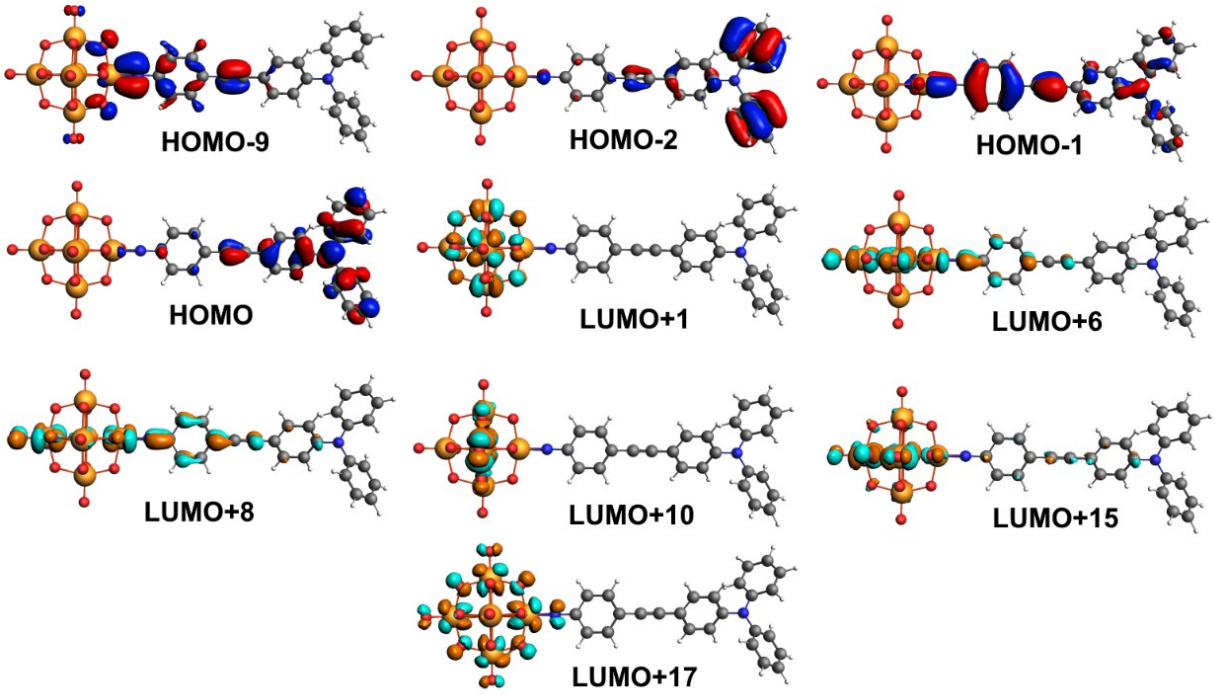

Fig. S6 Orbitals involved in the UV-vis transitions of compound **2**.

Analysis of Table S4 and Fig. S4 reveals three groups of transitions:
Organic (inc. bridge)-to-POM: Highly dipolar and moderately strong, total normalised f_{os} = 0.259
Donor to-POM/imido-aryl: Highly dipolar and moderately strong, total f_{os} = 0.259
Organic (inc. bridge)-to-POM/imido-aryl: Significant dipolar character, strong, total normalised f_{os} = 0.332

Table S5 Calculated Gas Phase Electronic Transitions of Compound **3**

Transition Energy / eV	f_{os}	Normalised f_{os}	Orbital contributions
1.47	0.1803	0.1088	HOMO → LUMO+6 (76%; 0.083) HOMO → LUMO+7 (13%; 0.0141) HOMO → LUMO+8 (9%; 0.009) HOMO → LUMO+4 (8%; 0.008)
2.04	0.4655	0.2808	HOMO → LUMO+8 (64%; 0.180) HOMO → LUMO+11 (10%; 0.028) HOMO → LUMO+6 (6%; 0.017) HOMO-1 → LUMO+6 (5%; 0.014)
2.36	0.1500	0.0904	HOMO-1 → LUMO+6 (71%; 0.064) HOMO-1 → LUMO+8 (12%; 0.011) HOMO-1 → LUMO+7 (10%; 0.009)
3.00	0.6471	0.3904	HOMO-1 → LUMO+8 (60%; 0.234) HOMO-1 → LUMO+6 (6%; 0.023) HOMO-1 → LUMO+15 (6%; 0.023) HOMO-1 → LUMO+11 (5%; 0.020) HOMO → LUMO+8 (3%; 0.012)
3.39	0.2146	0.1295	HOMO-5 → LUMO+7 (46%; 0.060) HOMO-1 → LUMO+15 (15%; 0.019) HOMO-6 → LUMO+7 (6%; 0.008) HOMO-8 → LUMO+1 (6%; 0.008) HOMO-1 → LUMO+16 (5%; 0.006)

[a] f_{os} normalised to the sum of the f_{os} all of the calculated transitions as 1. [b] Significant contributing orbital-to-orbital transitions with weighting (% and normalised f_{os}).

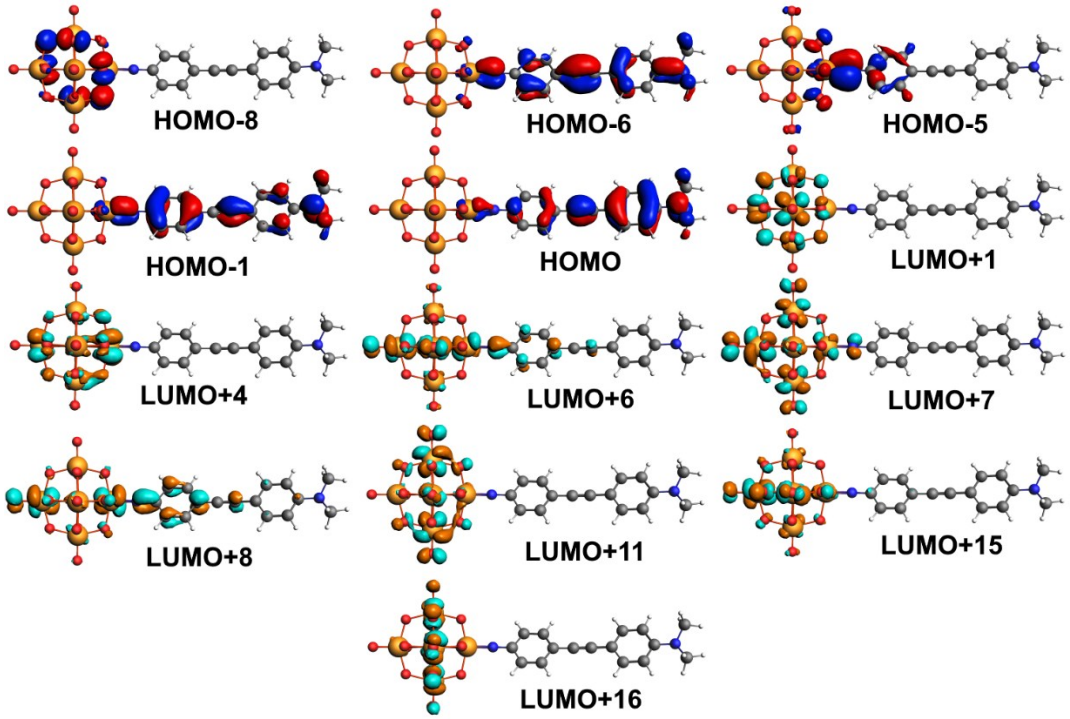

Fig. S7 Orbitals involved in the UV-vis transitions of compound **3**.

Analysis of Table S5 and Fig. S5 reveals two groups of transitions:
Organic (inc. bridge)-to-POM: Highly dipolar and moderately strong, total normalised f_{os} = 0.195
Organic (inc. bridge)-to-POM/imido-aryl: Significant dipolar character, very strong, total normalised f_{os} = 0.647.

^{1}H-NMR Spectra

Proton NMR spectra obtained of **P1** to **P3**, **1** and **2** are displayed over the following pages

9-(4-iodophenyl)-9H-carbazole (P1)

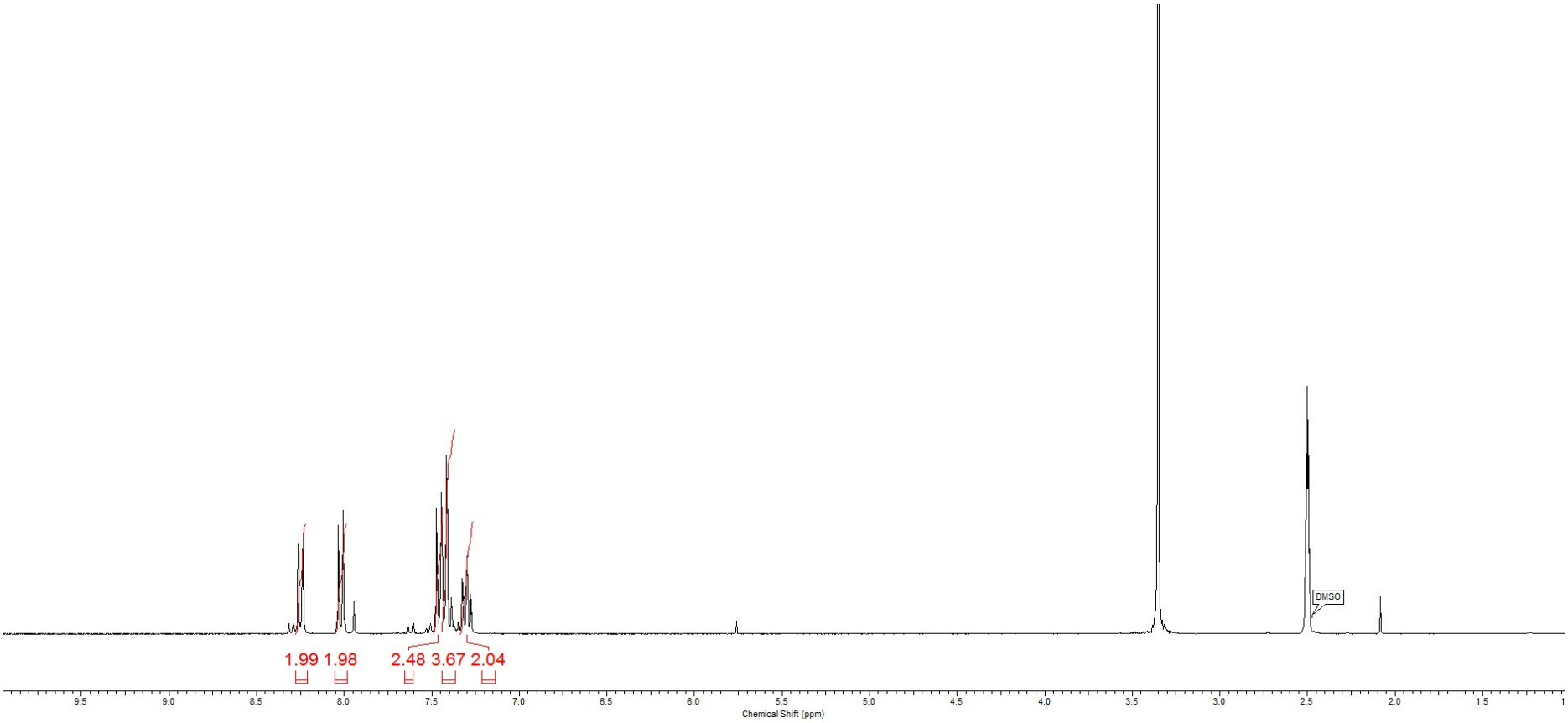

4-{[4-(9H-carbazol-9-yl)phenyl]ethynyl}aniline (P2)

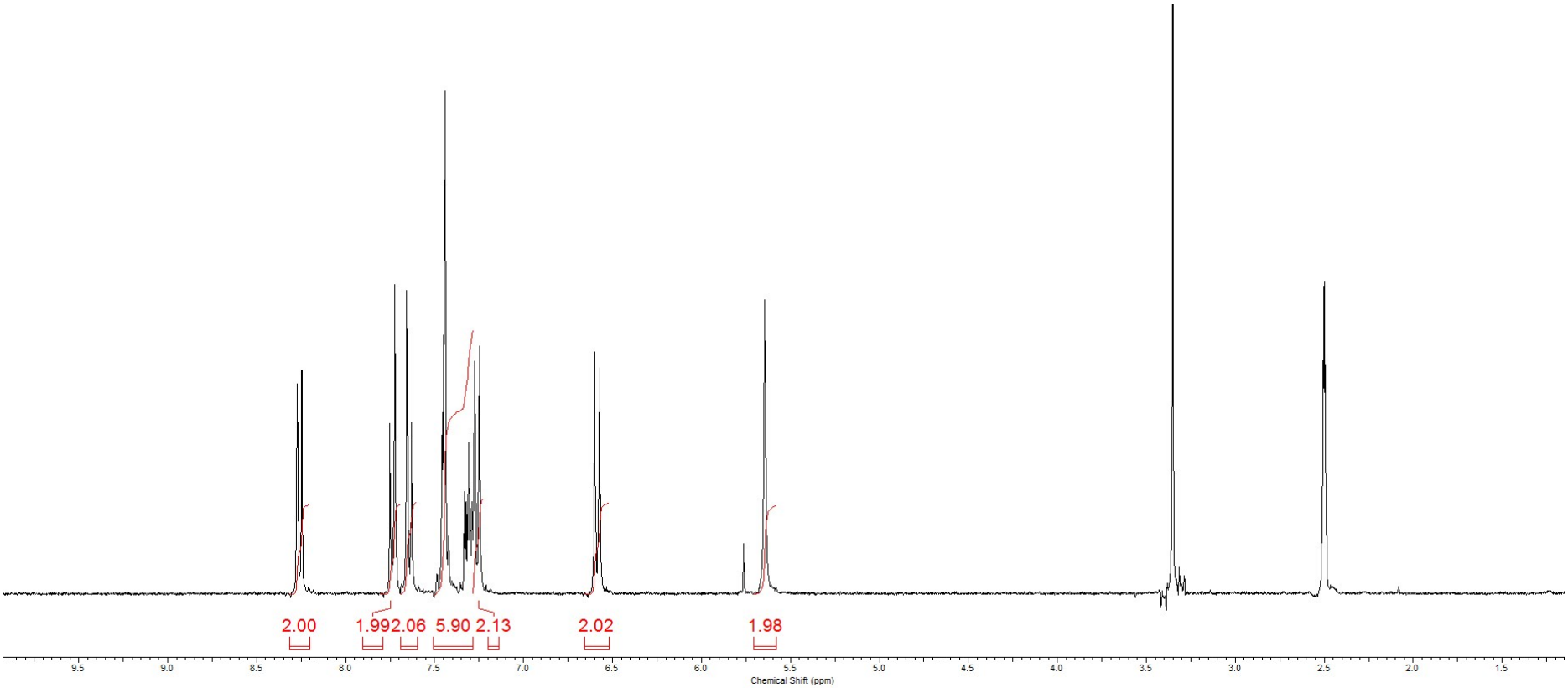

4-[(4-aminophenyl)ethynyl]-N,N-diphenylaniline (P3)

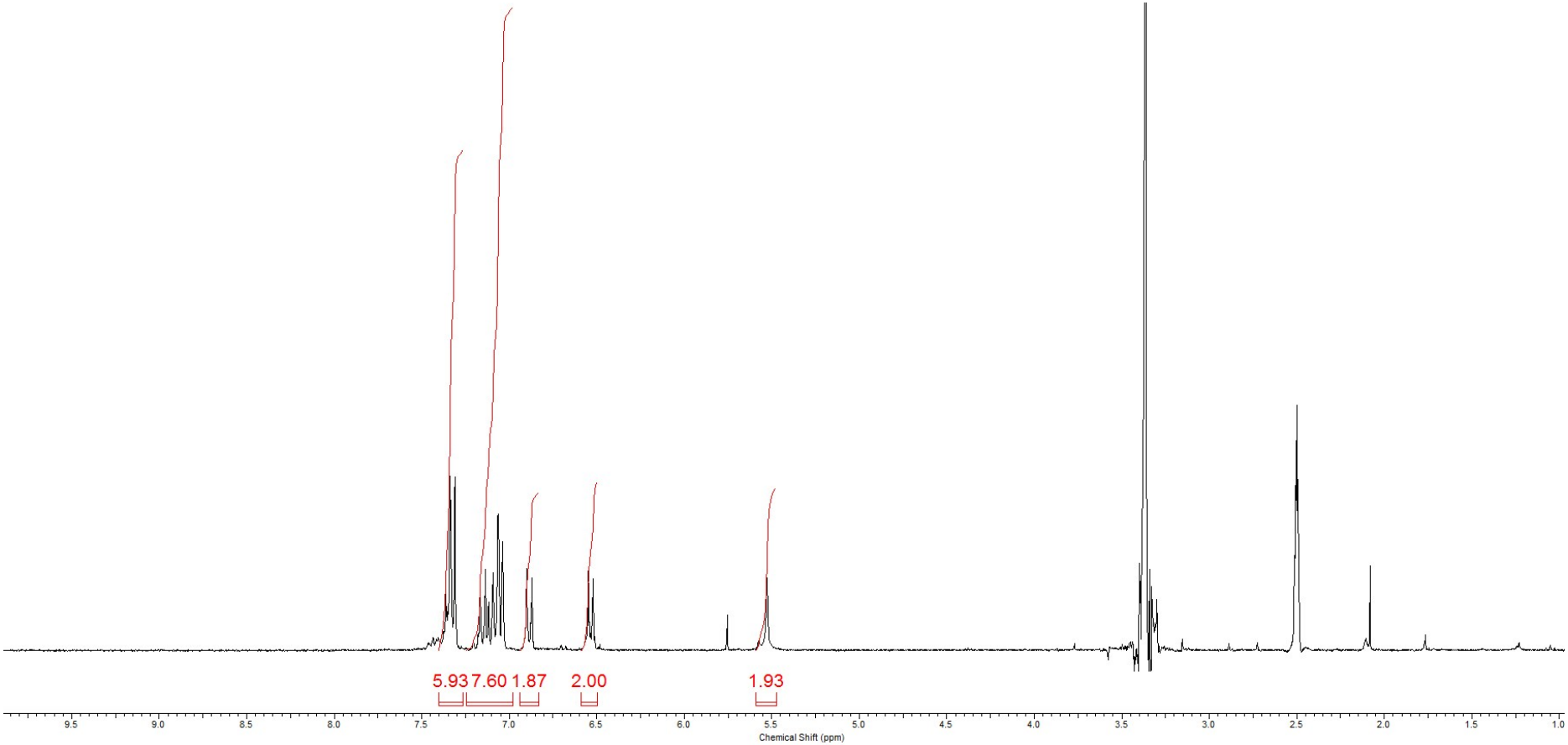

$[(C_4H_9)_4N]_2[Mo_6O_{18}N_2C_{26}H_{16}]$ (1)

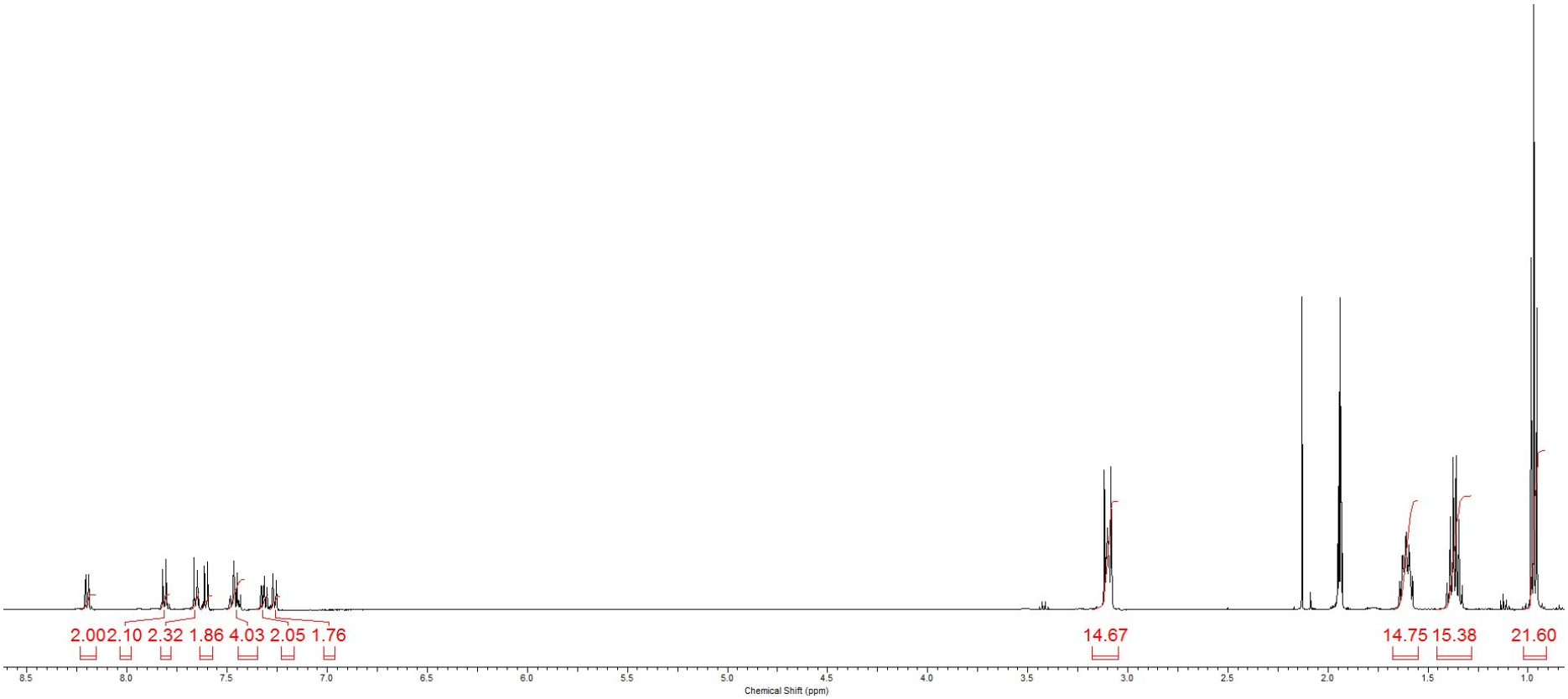

$[(C_4H_9)_4N]_2[Mo_6O_{18}N_2C_{26}H_{18}]$ (2)

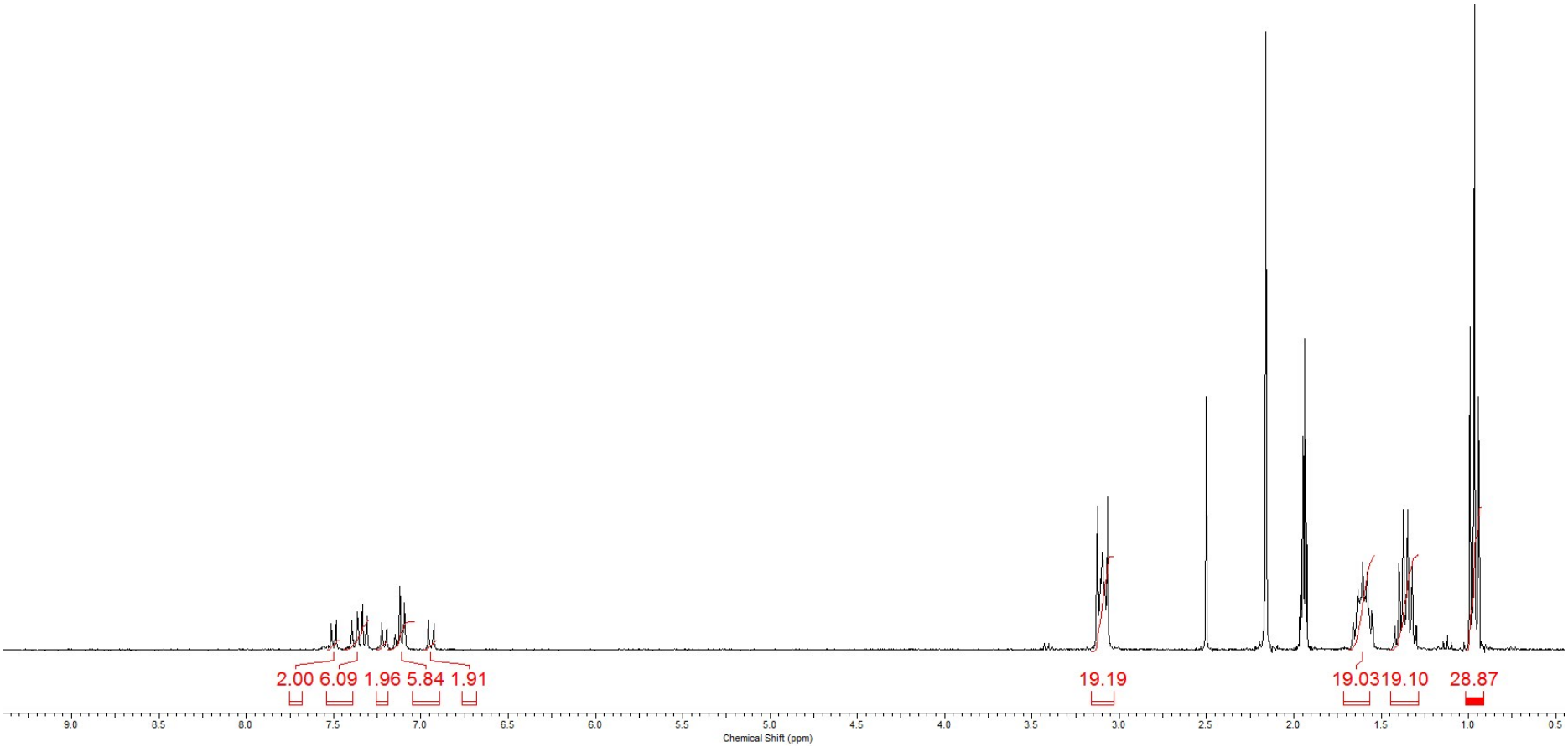

References

1. W. L. F. Armarego and C. L. L. Chai, *Purification of laboratory chemicals*; 6th ed.; Elsevier/Butterworth-Heinemann: Amsterdam; Boston, 2009.

2. W. G. Klemperer, *Inorg. Synth.* 1990, **27**, 71.

3. I. Bar-Nahum, K. V. Narasimhulu, L.Weiner and R. Neumann, *Inorg Chem.* 2005, **44**, 4900.

4. S. K. Ibrahim, Ph.D Thesis, University of Sussex, 1992.

5. (a) A. Al-Yasari, N. Van Steerteghem, H. El Moll, K. Clays and J. Fielden, *Dalton Trans.* 2016, **45**, 2818. (b) A. Al-Yasari, N. Van Steerteghem, H. Kearns, H. El Moll, K. Faulds, J. A. Wright, B. S. Brunschwig, K. Clays and J. Fielden, *Inorg. Chem.* 2017, **17**, 10181.

6. *CrysAlisPro* (Version 1.171.36.21), Agilent Technologies, Inc.; Santa Clara: CA, United States, 2012.

7. *CrystalClear-SM Expert* (Version 3.1 b27), Rigaku Corporation; Tokyo: Japan, 2013.

8. G. M. Sheldrick, *SHELXS-2014*, Programs for Crystal Structure Analysis (Release 2014-7); University of Göttingen: Göttingen, Germany, 2014.

9. L. J. Farrugia, *J. Appl. Cryst.* 1999, **32**, 837.

10. O. V. Dolomanov, L. J. Bourhis, R. J. Gildea, J. A. K. Howard and H. Puschmann, *J. Appl. Cryst.* 2009, 42, 339.

11. G. M. Sheldrick, *SHELXL-2014*, Programs for Crystal Structure Analysis (Release 2014-7); University of Göttingen: Göttingen, Germany, 2014.

12. L. J. Farrugia, *J. Appl. Cryst.* 1997, **30**, 565.

13. (a) K. Clays and A. Persoons, *Phys. Rev. Lett*. 1991, **66**, 2980. (b) K. Clays and A. Persoons, *Rev. Sci. Instrum*. 1992, **63**, 3285. (c) E. Hendrickx, K. Clays and A. Persoons, *Acc. Chem. Res.* 1998, **31**, 675.

14. (a) G. Olbrechts, R. Strobbe, K. Clays and A. Persoons, *Rev. Sci. Instrum*. 1998, **69**, 2233. (b) G. Olbrechts, K. Wostyn, K. Clays and A. Persoons, *Optics Lett*. 1999, ***24***, 403. (c) K. Clays, K. Wostyn, G. Olbrechts, A. Persoons, A. Watanabe, K. Nogi, X.-M. Duan, S. Okada, H. Oikawa, H. Nakanishi, H. Vogel, D. Beljonne and J.-L. Brédas, *J. Opt. Soc. Am. B* 2000, **17**, 256. (d) E. Franz, E. C. Harper, B. J. Coe, P. Zahradnik, K. Clays and I. Asselberghs, *Proc. SPIE–Int. Soc. Opt. Eng*. 2008, **6999**, 699923-1–699923-11.

15. J. Campo, F. Desmet, W. Wenseleers and E. Goovaerts, *Opt. Express* 2009, **17**, 4587.

16. (a) Y. K. Shin, B. S. Brunschwig, C. Creutz and N. Sutin, *J. Phys. Chem.* 1996, **100**, 8157. (b) B. J. Coe, J. A. Harris and B. S. Brunschwig, *J. Phys. Chem. A* 2002, **106**, 897.

17. (a) W. Liptay, in *Excited States*, Vol. 1; Ed. E. C. Lim, Academic Press, New York, 1974, pp. 129–229. (b) G. U. Bublitz and S. G. Boxer, *Annu. Rev. Phys. Chem.* 1997, **48**, 213. (c) F. W. Vance, R. D. Williams and J. T. Hupp, *Int. Rev. Phys. Chem.* 1998, **17**, 307. (d) B. S. Brunschwig, C. Creutz and N. Sutin, *Coord. Chem. Rev.* 1998, **177**, 61.

18. (a) G. Te Velde, F. M. Bickelhaupt, E. J. Baerends, C. Fonseca Guerra, S. J. A. van Gisbergen, J. G. Snijders and T. Ziegler, *J. Comput. Chem.* 2001, **22**, 931. (b) C. Fonseca Guerra, J. G. Snijders, G.

Te Velde and E. Baerends, *J. Theor. Chem. Acc.* 1998, **99**, 391. (c) ADF2017.110, SCM, Theoretical Chemistry, Vrije Universiteit, Amsterdam, The Netherlands, http://www.scm.com.

19. E. van Lenthe, E. J. Baerends and J. G. Snijders, *J. Chem. Phys.* 1993, **99**, 4597.

20. A. D. Becke, *Phys. Rev. A* 1988, **38**, 3098.

21. J. P. Perdew, *Phys. Rev. B* 1986, **33**, 8822.

22. S. J. A. van Gisbergen, J. G. Snijders and E. J. Baerends, *Comput. Phys. Commun.* 1999, **118**, 119.

23 (a) O. V. Gritsenko, P. R. T. Schipper and E. J. Baerends, *Chem. Phys. Lett.* 1999, **302**, 199; (b) P. R. T. Schipper, O. V. Gritsenko, S. J. A. van Gisbergen and E. J. Baerends, *J. Chem. Phys.* 2000, **112**, 1344.

24. M. R. S. A. Janjua, *Inorg. Chem.* 2012, **51**, 11306.

25. A. Willetts, J. E. Rice and D. M. Burland, *J. Chem. Phys.* 1992, **97**, 7590.